Photodissociation Dynamics of $C_6H_xF_{6-x}$ ($x = 1-4$) at 193 nm†

Ming-Fu Lin,‡ Yuri A. Dyakov,‡ Sheng Hsien Lin,‡,§ Yuan T. Lee,‡,§ and Chi-Kung Ni*,‡

Institute of Atomic and Molecular Sciences, Academia Sinica, P.O. Box 23-166, Taipei, Taiwan, and Chemistry Department, National Taiwan University, Taipei, Taiwan

Received: May 31, 2004; In Final Form: September 5, 2004

Photodissociation of fluorine-substituted benzenes, including 1,3-difluorobenzene, 1,2,4-trifluorobenzene, 1,2,4,5-tetrafluorobenzene, and pentafluorobenzene, at 193 nm under collision-free conditions has been studied in separate experiments using multimass ion imaging techniques**.** HF elimination was found to be the major dissociation channel for all of these molecules. Small amounts of photofragments of $C_6H_3F_2$ and $C_6H_2F_3$ from 1,3-difluorobenzene and 1,2,4-trifluorobenzene, respectively, were also observed. They correspond to the minor dissociation channel of hydrogen elimination. Dissociation rates and fragment translational energy distributions obtained from experimental measurements suggest that HF and hydrogen elimination reactions occur in the ground electronic state. The potential energy surface obtained from ab initio calculations indicates that the four-center reaction in the ground electronic state is the major dissociation mechanism for the HF eliminations. A comparison with the RRKM calculation has been made.

I. Introduction

Phenyl halides are one of the aromatic compounds that has been studied extensively. Photodissociation of phenyl halides (−Cl, −Br, −I) shows a simple dissociation channel, i.e., halogen atom elimination. The simple dissociation channel can be rationalized from the fact that ultraviolet (UV) absorption of the phenyl halides (−Cl, −Br, −I) in the 190−250 nm range corresponds to the excitations of electrons of the phenyl ring and the nonbonding electrons of the halogen atoms. The nonbonding electron excitation of the halogen atoms leads to direct dissociation, an immediate release of halogen atoms on a repulsive surface. However, the excitation of the phenyl ring results in an excited state, stable with respect to dissociation. Dissociation occurs indirectly either through the coupling of the stable and repulsive state or after the internal conversion from an initially excited state to a lower electronic state. Statistical transition state theory has predicted that, given comparable preexponential factors for different bond fissions, the reaction pathway with the lowest energetic barrier should dominate the indirect dissociation. Since the C−X (X = Cl, Br, I) bond energy is relatively small, halogen atom elimination is expected to be the major channel in the indirect dissociation. Recent theoretical calculation[1] supports this simple picture, although it shows that more than one repulsive state can be involved in the dissociation process and the dissociation mechanism is complicated by the coupling of various electronic states.

In the photodissociation of iodobenzene,[2,3] bromobenzene,[3,4] chlorobenzene,[3,5−8] and *o*-, *m*-, and *p*-dichlorobenzene,[9−11] halogen atom elimination indeed has been found to be the only dissociation channel, and both direct and indirect dissociation have been observed. For the photodissociation of chlorotoluene at 193 nm, chlorine,[8,9,12,13] hydrogen, and CH_3 eliminations[14] were observed. The observation of hydrogen and CH_3 eliminations can be understood from the fact that the cleavages of the C−H bond and the C−C bond also have relatively low dissociation thresholds, and therefore they compete with the chlorine elimination in the indirect dissociation.

In comparison to the other phenyl halides, the photochemistry of fluorine-substituted benzenes has received little attention. Since fluorine is not an electronic chromophore in the range of 190−250 nm, UV absorption only correlates to the excitation of the phenyl ring. Therefore, an immediate release of the fluorine on a repulsive surface does not occur. In addition, the C−F bond has a very high dissociation threshold, and fluorine elimination from the ground state after internal conversion is not expected to occur. As a result, the dissociation mechanism in this photon energy region should be very different from those of the other phenyl halides. However, one would expect that the photodissociation mechanism of fluorobenzene could be similar to that of benzene, since both of them correlate to the excitation of the phenyl ring and the weakest chemical bond in both molecules is the C−H bond.

Recently, we have studied the photodissociation of fluorobenzene at 193 nm.[15] Dissociation occurs, as expected, after internal conversion to the electronic ground state. However, hydrogen elimination is only a minor dissociation channel. Instead, HF elimination was found to be the major channel. It is a four-center elimination mechanism, unlike the proposed three-center H_2 elimination mechanism in benzene.[16] In this work, we extend the study to the other fluorine-substituted benzenes. Photofragment translational energy distributions and dissociation rates were measured using multimass ion imaging techniques. Results are compared to the potential energy surfaces obtained from ab initio calculation and dissociation rates from statistical methods.

II. Experimental Section

The experiments have been described in detail elsewhere,[17] and only a brief description is given here. Fluorine-substituted benzene vapor was formed by flowing ultrapure helium at

* Author to whom correspondence should be addressed. E-mail: ckni@po.iams.sinica.edu.tw.

† Part of the special issue "George W. Flynn Festschrift".

‡ Academia Sinica.

§ National Taiwan University.

10.1021/jp047647g CCC: $30.25
Published on Web 01/27/2005

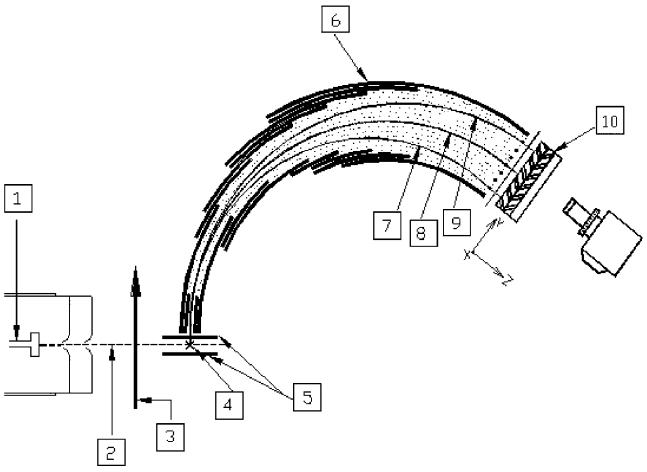

Figure 1. A schematic diagram of the multimass ion imaging detection system. (1) nozzle, (2) molecular beam, (3) photolysis laser beam, (4) VUV laser beam, (5) ion extraction plates, (6) mass spectrometer, simulation trajectories of $m/e = 16$ (7), 14 (8), and 12 (9), and (10) 2D ion detector.

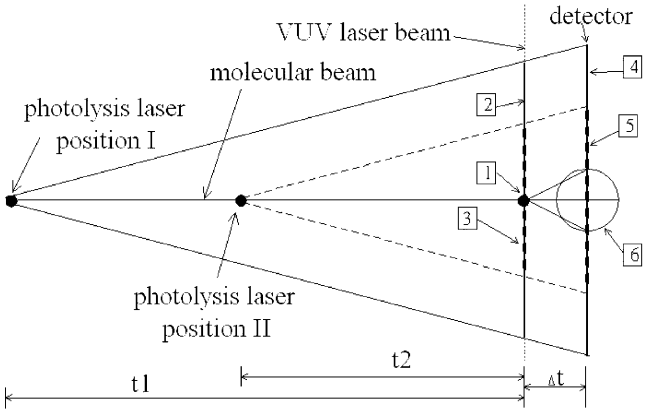

Figure 2. Relationship between the lengths of the images that result from different crossing points of the photolysis laser beam with the molecular beam. The disklike image from the dissociation after ionization is also shown. (1) Solid circle represents the crossing point of the molecular beam and the VUV laser beam, where the dissociative ionization occurs. The disklike image (6) is from these dissociative ionizations. (2) Thick solid line and (3) thick dashed line represent the lengths of the fragment-ion distributions created by the VUV laser photoionization from the photolysis laser at position I and position II, respectively. The line-shape images, represented by (4) the thick solid line and (5) the thick dashed line, are from these fragment-ion distributions. The t_1 and t_2 represent two different delay times between the photolysis laser pulse and the VUV laser pulse according to two different photolysis laser positions. Δt is the flight time of the fragment ion in the mass spectrometer.

pressures of 400 Torr through a reservoir filled with liquid sample at 10 °C. The fluorine-substituted benzene/helium mixture was then expanded through a 500 μm pulsed nozzle at temperature 60 °C to form the molecular beam. The low temperature at the sample reservoir, low pressure of carrier gas, and the high temperature at the nozzle can avoid the generation of clusters. Molecules in the molecular beam were photodissociated by an UV photolysis laser pulse (Lambda Physik Compex 205, ~20 ns pulse duration). Due to the recoil velocity and center-of-mass velocity, the fragments were expanded to a larger sphere on their flight to the VUV laser beam, then ionized by a VUV laser pulse. The distance and time delay between the VUV laser pulse and the photolysis laser pulse were set such that the VUV laser beam passed through the center-of-mass of the dissociation products and generated a line segment of photofragment ions through the center-of-mass of the dissociation products by photoionization. The length of the segment was proportional to the fragment recoil velocity in the center-of-mass frame multiplied by the delay time between the photolysis and the ionization laser pulses. To separate the different masses within the ion segment, a pulsed electric field was used to extract the ions into a mass spectrometer after ionization. While the mass analysis was being executed in the mass spectrometer, the length of each fragment-ion segment continued to expand in the original direction according to its recoil velocity. At the exit port of the mass spectrometer, a two-dimensional (2D) ion detector was used to detect the ion positions and intensity distribution. In this two-dimensional detector, one direction was the recoil velocity axis and the other was the mass axis. The schematic diagram of the experimental set up is shown in Figure 1.

According to the velocity of the molecular beam, it was necessary to change the distance between the photolysis laser beam and the VUV laser beam to match the delay time between these two laser pulses to ensure that the ionization laser would pass through the center-of-mass of the products. The change of the distance between the two laser beams changed the length of the fragment-ion segment in the image. The relationship between the length of the ion image and the position of the photolysis laser is illustrated in Figure 2. If the molecules were not dissociated after the absorption of the UV photons, then these high-internal-energy molecules would remain within the molecular beam. They flew with the same velocity (molecular beam velocity) to the ionization region and were ionized by the VUV laser. The wavelength of the VUV laser in this experiment was set at 118.2 nm such that the photon energy was only large enough to ionize parent molecules. The dissociation of parent molecule cations would not occur with the energy left after the VUV laser ionization. However, the dissociation occurred following the VUV laser ionization for those molecules that absorbed a UV photon without dissociation. The ion image of the dissociative ionization was different from the image due to the dissociation products of neutral parent molecules. Since ionization and dissociation occurred at the same position, the image of dissociative ionization was a 2D projection of the photofragment ion's 3D recoil velocity distribution. It was very similar to the image from the conventional ion imaging techniques and was a disklike image rather than a line-shape image. From the shape of the image and its change with the delay time, the image from the dissociation of neutral molecules can easily be distinguished from the dissociative ionization image.

The dissociation rate can be obtained from the product growth with respect to the delay time between the pump and the probe lasers. However, accurate measurement can be obtained only when the dissociation rate is fast enough before the parent molecules and fragments fly out of the detection region due to the molecular beam velocity and recoil velocity, respectively. Another approach is to measure the disappearance rate of the parent molecules; that is the intensity change of the disklike images at various delay times along the molecular beam.[18] In this work, the dissociation rates were obtained from both methods.

III. Result and Discussion

Fragment ions of $m/e = 63$, 70, 81, 88, 94, and 113 were observed from the photodissociation of 1,3-difluorobenzene at 193 nm. The shapes of the images of $m/e = 63$, 70, 81, and 88 are all disklike. Some of them are shown in Figure 3, parts a

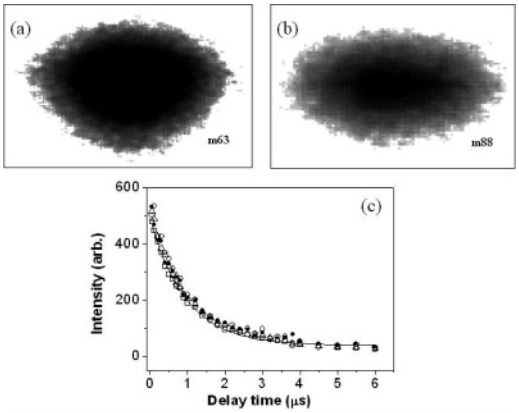

Figure 3. Disklike images of (a) $m/e = 63$ and (b) $m/e = 88$. (c) Decay of the disklike image as a function of the delay time between the pump and the probe laser pulses. Open square, $m/e = 88$; open circle, $m/e = 81$; solid circle, $m/e = 70$; open triangle, $m/e = 63$. A decay rate of $(1.0 \pm 0.1) \times 10^6$ s^{-1} was obtained from the fitting of the experimental data.

and b. These images must result from the dissociative ionization of undissociated difluorobenzene after absorption of a 193 nm photon. Some of these cation dissociation channels have been observed in previous studies.[19] The dissociation rate of the neutral excited difluorobenzene molecules due to the 193 nm photon excitation was measured from the intensity change of these disklike images at various delay times. A dissociation rate of $(1.0 \pm 0.1) \times 10^6$ s^{-1}, corresponding to the lifetime of 1.0 μs, was obtained from the intensity decay of $m/e = 63$, 70, 81, and 88. They are shown in Figure 3c.

A fragment ion, $m/e = 94$ ($C_6H_3F^+$), has the largest ion intensity, and it has a line-shape image. As the delay time between the pump and the probe laser pulses increased, the length of the image increased rapidly, as shown in Figure 4, parts a and b. This is the C_6H_3F fragment that resulted from the dissociation of neutral excited 1,3-difluorobenzene, corresponding to the HF elimination. A dissociation rate of $(1.0 \pm 0.3) \times 10^6$ s^{-1} was obtained from the product growth with respect to the delay time between the pump and the probe laser pulses, as shown in Figure 4c. The uncertainty of this rate measurement is large due to the fast escape of the product from the detection region. However, the similar dissociation rates of $m/e = 94$ and the other disklike images indicate that they must be from the same electronic state.

The photofragment translational energy distribution of the HF elimination is shown in Figure 4d. The average released translational energy is large, and the peak of the distribution is located at 29 kcal/mol. The slow dissociation rate and the large translational energy release similar to that of fluorobenzene[15] suggest that fluorobenzene and difluorobenzene must have a similar dissociation mechanism, i.e., dissociation occurs in the ground state with an exit barrier after internal conversion.

The fragment-ion intensity decay of $m/e = 113$, corresponding to a dissociation rate of $(1.0 \pm 0.3) \times 10^6$ s^{-1}, was obtained, as shown in Figure 5. The value of the rate indicates that it comes the same electronic state as that of the HF elimination channel. The nonzero intensity of $m/e = 113$ ($C_6H_3F_2^+$) at long delay time suggests the existence of the hydrogen elimination channel of neutral excited fluorobenzene. Although $m/e = 113$ can be separated from the parent molecule of $m/e = 114$ in a time-of-flight mass spectrum, unfortunately the image of $m/e = 113$ showed strong interference by the parent ion due to the small $m/e = 113$ signal and large parent ion intensity. The fragment-ion intensity of $C_6H_3F_2^+$ is 27 times smaller than that of C_6H_3F. This value has been corrected for the fragment velocity effect (mainly for the HF elimination channel). The branching ratios can be obtained directly from the normalization of these values by the ionization cross sections at this wavelength. Although we do not have the ionization cross sections for these fragments at this moment, the large difference of the ion intensities between these two fragments indicates that HF elimination is the major channel.

The 1,3-difluorobenzene potential energy curves for various dissociation channels obtained by calculations are shown in Figure 6. In the calculation, the geometries were optimized by B3LYP/6-31G* and the energies were calculated by the G3 scheme. The potential energy curves are found to be very similar to that of fluorobenzene. Fluorine elimination occurs through the C−F bond cleavage, which is illustrated by a high dissociation threshold. Hydrogen elimination can occur from three different positions of the aromatic ring, resulting in slightly different energies. There are two different dissociation mechanisms for the HF eliminations. One is the three-center elimination, and the other is the four-center elimination. The three-center HF elimination starts from the 1,2 or 1,6 hydrogen atom shift and then HF elimination through transition state TS3a or TS3b, producing 2-fluorobenzyne and 3-fluorobenzyne, respectively. The energy difference between the transition state TS3a and TS3b and the energy difference between the final product 2-fluorobenzyne and 3-fluorobenzyne are both very small. The differences are only 0.9 and 1.6 kcal/mol, respectively. These two pathways of three-center elimination have similar dissociation energy and barrier heights. H_2 elimination also occurs through the similar three-center elimination. One common property of these three-center elimination channels is that the dissociation barriers are as high as ~120 kcal/mol. HF four-center elimination also has two pathways, corresponding to two different HF elimination positions. However, both HF four-center eliminations have very low barriers. They are only 92−96.9 kcal/mol. They are the channels that dominate the photodissociation of 1,3-difluorobenzene at this wavelength. The geometries of 2-C_6H_3F and HF in the transition state TS4a are very close to the geometries of final products, 2-C_6H_3F and HF, respectively. This transition state has the late barrier characteristic. A more quantitative description of the late barrier characteristic can be found from the distortion energy. The distortion energy is defined as the energy difference between the final products P1 and the transition state TS4a without considering the interaction between 2-C_6H_3F and HF in the transition state. Basically, it is the energy due to the geometric difference of both C_6H_3F and HF between the final product and the transition state. The distortion energy was found to be only 9.6 kcal/mol, compared to the large exit barrier height of 22.6 kcal/mol in this channel. This strongly indicates the late barrier characteristic. Similar values of 10.9 and 25.7 kcal/mol for distortion energy and exit barrier height were also found in the transition state TS4b and final products P2. These values suggest that most of the 1,3-difluorobenzene dissociates through HF four-center elimination due to the low barrier height and the kinetic energy release is large because of the similar geometries between transition states and final products as well as the large exit barrier heights.

The dissociations of 1,3-difluorobenzene in the ground electronic state are unimolecular reactions, and they can be characterized with RRKM theory. We used the potential energy surface obtained from a G3 level calculation and performed the RRKM calculation for various reaction rates. The dissociation rates of fluorine elimination and hydrogen eliminations from

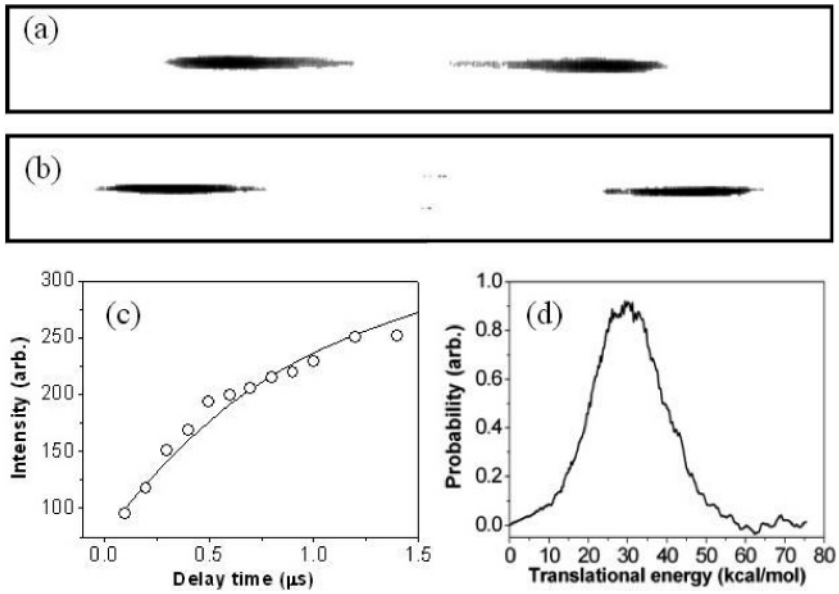

Figure 4. Fragment-ion images of $m/e = 94$ at the delay times of (a) 12 μs and (b) 20 μs. (c) Product growth of $m/e = 94$ with respect to the delay time. (d) Photofragment translational energy distribution of reaction $C_6H_4F_2 + h\nu \rightarrow C_6H_3F + HF$.

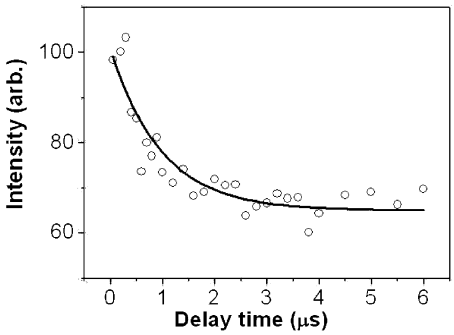

Figure 5. The intensity decay of $m/e = 113$ as a function of delay time between the pump and the probe laser pulses.

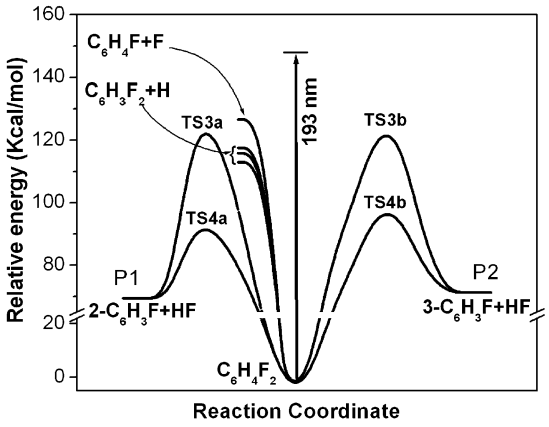

Figure 6. Potential curve for various dissociation channels of 1,3-difluorobenzene.

three different positions were found to be 5.88×10^1, 1.89×10^3, 3.89×10^3, and 1.3×10^4 s^{-1}, respectively. For three-center elimination, the results of the RRKM calculation show that the dissociation rates through TS3a and TS3b are 4.1×10^0 and $7.2 \times 10^0 s^{-1}$, respectively. The dissociation rate for the H_2 three-center elimination is 4.1×10^0 s^{-1}. HF four-center eliminations through TS4a and TS4b have a rate of 5.0×10^5 and 1.3×10^5 s^{-1}, respectively. The total dissociation rate of 1,3-difluorobenzene is 6.4×10^5 s^{-1}, and the branching ratio between HF elimination and hydrogen elimination is about 97:3. Their values are very close to the experimental results and support the four-center elimination mechanism.

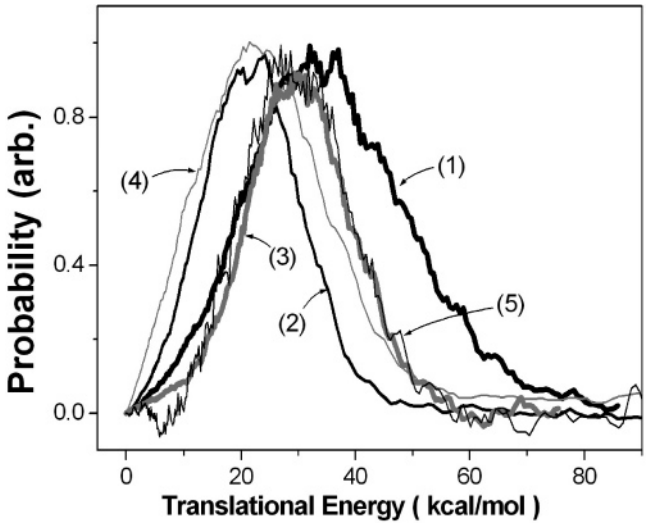

Figure 7. Photofragment translational energy distribution of $C_6H_{6-x}F_x + h\nu \rightarrow C_6H_{5-x}F_{x-1} + HF$. The numbers in parentheses represent the numbers of the fluorine atoms. Data for C_6H_5F is from ref 15.

Similar dissociation properties were also observed in the other fluorine-substituted benzenes, including 1,2,4-trifluorobenzene, 1,2,4,5-tetrafluorobenzene, and pentafluorobenzene. HF elimination is the dominant channel for these molecules, and the hydrogen elimination channel was only observed in trifluorobenzene as a minor channel. The translational energy release of the HF elimination channel is large for all of these molecules, as shown in Figure 7. The dissociation rates obtained from the decay of disklike images as well as from the product growth for each fluorine-substituted benzene are listed in Table 1 for the comparison with results from the RRKM calculations. The experimental results demonstrate that the dissociation rates decrease with the increase of the fluorine atom number. It can be rationalized from the fact that the number of low vibrational frequency modes increase as the number of the fluorine atom increases. As a result, the density of the state increases rapidly, and the dissociation rate decreases. The change of the dissociation rates with the number of fluorine atoms is consistent with

TABLE 1

reaction	calculation: barrier[e]	calculation: dissociation E[e]	calculation: distortion E[e]	calculation: rate[f]	expt
$C_6H_5F \rightarrow C_6H_5 + F$		125.9		1.8×10^2	
$C_6H_5F \rightarrow C_6H_4F + H$[a]		112.1−114.3		2.4×10^4	0.04[g]
$C_6H_5F \rightarrow C_6H_4 + HF$[b]	119.8	69.4		8×10^1	
$C_6H_5F \rightarrow C_6H_4 + HF$[c]	94.7	69.4	11.2	4.6×10^5	
				total = 4.8×10^5	8.3×10^5[f]
1,3-$C_6H_4F_2 \rightarrow C_6H_4F + F$		126.2		5.9×10^1	
1,3-$C_6H_4F_2 \rightarrow C_6H_3F_2 + H$[a]		113−117.6		1.9×10^3	
1,3-$C_6H_4F_2 \rightarrow$ 3-$C_6H_3F + HF$[b]	123.4	69.4		4.1×10^0	
1,3-$C_6H_4F_2 \rightarrow$ 3-$C_6H_3F + HF$[c]	92.0	69.4	9.6	5.0×10^5	0.04[g]
1,3-$C_6H_4F_2 \rightarrow$ 2-$C_6H_3F + HF$[b]	122.5	71.2		7.2×100^5	
1,3-$C_6H_4F_2 \rightarrow$ 2-$C_6H_3F + HF$[c]	96.9	71.2	10.9	1.3×10^5	
				total = 5.3×10^5	1.0×10^6[f]
1,2,4-$C_6H_3F_3 \rightarrow$ 3,4-$C_6H_3F_2 + F$[d]		125−126.2		2.9×10^1	
1,2,4-$C_6H_3F_3 \rightarrow C_6H_2F_3 + H$[a]		115.7−118		2.1×10^3	
1,2,4-$C_6H_3F_3 \rightarrow$ 2,5-$C_6H_2F_2 + HF$[b]	120.6	67.6		4.8×10^0	
1,2,4-$C_6H_3F_3 \rightarrow$ 2,5-$C_6H_2F_2 + HF$[c]	94.6	67.6	11.1	1.2×10^5	
1,2,4-$C_6H_3F_3 \rightarrow$ 2,4-$C_6H_2F_2 + HF$[b]	117.7	66.9		2.3×10^1	
1,2,4-$C_6H_3F_3 \rightarrow$ 2,4-$C_6H_2F_2 + HF$[c]	96.6	66.9	13.2	7.4×10^4	0.02[g]
1,2,4-$C_6H_3F_3 \rightarrow$ 2,3-$C_6H_2F_2 + HF$[b]	121.5	69.9		3.2×10^0	
1,2,4-$C_6H_3F_3 \rightarrow$ 2,3-$C_6H_2F_2 + HF$[c]	91.4	69.9	9.1	3.2×10^5	
1,2,4-$C_6H_3F_3 \rightarrow$ 3,4-$C_6H_2F_2 + HF$[b]	122.6	71.0		2.0×10^0	
1,2,4-$C_6H_3F_3 \rightarrow$ 3,4-$C_6H_2F_2 + HF$[c]	96.2	71.0	10.6	7.9×10^4	
				total = 5.9×10^5	4.7×10^5[f]
1,2,4,5-$C_6H_2F_4 \rightarrow C_6H_2F_3 + F$		125.1		1.1×10^1	
1,2,4,5-$C_6H_2F_4 \rightarrow C_6HF_4 + H$		118.5		2.6×10^2	
1,2,4,5-$C_6H_2F_4 \rightarrow C_6HF_3 + HF$[b]	118.8	67.7		3.8×10^0	0.00[g]
1,2,4,5-$C_6H_2F_4 \rightarrow C_6HF_3 + HF$[c]	93.4	67.7	10.4	9.3×10^4	
				total = 9.3×10^4	2.3×10^5[f]
$C_6HF_5 \rightarrow C_6HF_4 + F$[d]		123.6−124.4		9.7×10^0	
$C_6HF_5 \rightarrow C_6F_4 + H$		119.0		9.6×10^1	
$C_6HF_5 \rightarrow C_6F_4 + HF$[b]	119.2	67.0		8.8×10^{-1}	0.00[g]
$C_6HF_5 \rightarrow C_6F_4 + HF$[c]	93.9	67.0	11.1	4.1×10^4	
				total = 4.1×10^4	7.7×10^4[f]

[a] Includes hydrogen elimination from various positions. [b] Three-center elimination. [c] Four-center elimination. [d] Includes fluorine elimination from various positions. [e] In kcal/mol. [f] In s^{-1}. [g] Ratio of heavy-fragment-ion intensities between all various positions of hydrogen elimination and HF elimination.

the RRKM calculation. However, the potential energy surfaces do not change with the number of fluorine atoms, especially for the major dissociation channel of the HF four-center elimination. The exit barrier heights and transition state distortion energies for the HF four-center elimination almost remain at the same values, as shown in Table 1. This explains why the four-center HF elimination is the major channel for all of the fluorine-substituted benzenes and they have a large translational energy release. The branching ratios of the hydrogen elimination also decrease with the increase of the number of fluorine atoms. They are also consistent with the RRKM calculation.

In conclusion, we demonstrate that dissociation of all fluorine-substituted benzenes occur in the ground electronic state after internal conversion. HF elimination is the dominant dissociation channel, and the dissociation mechanism is a four-center elimination. The amount of the translational energy release is large, and it does not change significantly with the number of the substituted fluorine atoms. However, the dissociation rates decrease with the increase of fluorine atoms. Both of them can be rationalized from the potential energy surfaces and the RRKM calculation. In comparison to the other phenyl halides, fluorine-substituted benzenes show significantly different dissociation properties, and they are the only phenyl halides that produce two closed-shell fragments in this photon energy region.

Acknowledgment. The work was supported by the National Science Council, Taiwan, under contract NSC 92-2113-M-001-015.

References and Notes

(1) Liu, Y. J.; Persson, P.; Lunell, S. *J. Phys. Chem. A* **2004**, *108*, 2339.

(2) Dzvonik, M.; Yang, S.; Bersohn, R. *J. Chem. Phys.* **1974**, *61*, 4408.

(3) Freedom, A.; Yang, S. C.; Kawasaki, M.; Bersohn, R. *J. Chem. Phys.* **1980**, *72*, 1028.

(4) Zhang, H.; Zhu, R. S.; Wang, G. J.; Han, K. L.; He, G. Z.; Lou, N. Q. *J. Chem. Phys.* **1999**, *110*, 2922.

(5) Han, K. L.; He, G. Z.; Lou, N. Q. *Chem. Phys. Lett.* **1993**, *203*, 509.

(6) Wang, G. J.; Zhu, R. S.; Zhang, H.; Han, K. L.; He, G. Z.; Lou, N. Q. *Chem. Phys. Lett.* **1998**, *288*, 429.

(7) Ichimura, T.; Mori, Y.; Shinohara, H.; Nishi, N. *Chem. Phys.* **1994**, *189*, 117.

(8) Ichimura, T.; Mori, Y.; Shinohara, H.; Nishi, N. *Chem. Phys. Lett.* **1985**, *122*, 51.

(9) Ichimura, T.; Mori, Y.; Shinohara, H.; Nishi, N. *J. Chem. Phys.* **1997**, *107*, 835.

(10) Satyapal, S.; Tasaki, S.; Bersohn, R. *Chem. Phys. Lett.* **1993**, *203*, 349.

(11) Ichimura, T.; Shimoda, A.; Kikuchi, T.; Kohso, Y.; Hikid, T.; Mori, Y. *J. Photochem.* **1985**, *31*, 157.

(12) Kawasaki, M.; Kasatani, K.; Sato, H.; Shinohara, H.; Nishi, N. *Chem. Phys.* **1984**, *88*, 135.

(13) Satyapal, S.; Tasaki, S.; Bersohn, R. *Chem. Phys. Lett.* **1993**, *203*, 349.

(14) Lin, M. F.; Huang, C. L.; Kislov, V. V.; Mebel, A. M.; Lee, Y. T.; Ni, C. K. *J. Chem. Phys.* **2003**, *119*, 7701.
(15) Huang, C. L.; Jiang, J. C.; Mebel, A. M.; Lee, Y. T.; Ni, C. K. *J. Am. Chem. Soc.* **2003**, *125*, 9814.
(16) Mebel, A. M.; Lin, M. C.; Chakraborty, D.; Park, J.; Lin, S. H.; Lee, Y. T. *J. Chem. Phys.* **2001**, *114*, 8421.
(17) Tsai, S. T.; Lin, C. K.; Lee, Y. T.; Ni, C. K. *Rev. Sci. Instrum.* **2001**, *72*, 1963.
(18) Tsai, S. T.; Lin, C. K.; Lee, Y. T.; Ni, C. K. *J. Chem. Phys.* **2000**, *113*, 67.
(19) Momigny, J.; Wirtz-Cordier, A. M. *Ann. Soc. Sci. Bruxelles*, **1962**, *76*, 164.